Enhanced resistance to proton irradiation of poly(dimethylsiloxane) resins through surface embedding of silica photonic crystals

David Lansade, Simon Lewandowski, Stéphanie Remaury, Guillaume Sierra, Stéphane Solé, Sophie Perraud, Stéphane Carlotti

Version of Record: https://www.sciencedirect.com/science/article/pii/S0141391020300951
Manuscript_c3aa6aa95f5bcd9216da5bf9d994ce81

Enhanced resistance to proton irradiation of poly(dimethylsiloxane) resins through surface embedding of silica photonic crystals

David Lansade[a,b,d], *Simon Lewandowski*[a], *Stéphanie Remaury*[b], *Guillaume Sierra*[c], *Stéphane Solé*[c], *Sophie Perraud*[b], *Stéphane Carlotti*[d,*]

[a] ONERA – The French Aerospace Lab, F31055 Toulouse, France

[b] CNES – French Aerospace Agency, 18 avenue Edouard Belin F-31401 Toulouse Cedex 9, France

[c] MAP Coatings, 2 rue Clément Ader 09100 Pamiers, France

[d] Univ. Bordeaux, CNRS, Bordeaux INP, LCPO, UMR 5629, F-33600, Pessac, France

*Corresponding author. E-mail address: stephane.carlotti@enscbp.fr

ABSTRACT

Poly(dimethylsiloxane) (PDMS) based resins are materials used in large amounts on spacecrafts and satellites. When such materials are exposed to proton irradiation, especially in geostationary environment, they tend to crack and turn yellow, this being detrimental to their operational status. Here we present the elaboration and ageing of hybrid materials made of the embedding of non- or vinyl-functionalized silica nanoparticles (SiO_2 NPs) assembled into a photonic crystal at the surface of a PDMS matrix. The influences of the size of the nanoparticles, the thickness of the crystal as well as the grafting density of vinyl moieties on the proton resistance of the materials were studied. The materials maintained the initial transparency of PDMS in a wide spectroscopic range. Transparency of the materials was evaluated using UV-vis-NIR spectroscopy before and after accelerated proton-induced ageing was carried out to simulate part of proton irradiation encountered in geostationary environment. Fourier Transformed Infra-Red-Attenuated Total Reflection (FTIR-ATR) experiments allowed comprehensive study of

the mechanisms leading to the stabilization of the materials in terms of cracking and yellowing. Stabilization in regards of cracking was revealed thanks to optical and scanning electron microscopy.

Keywords: proton irradiation, polymer stability, poly(dimethyl siloxane), silica nanoparticle, nanocomposite

INTRODUCTION

Study of interactions between charged particles and materials is of prime importance as these energetic particles may induce damages in materials through which they go. Silicon-based resins are widely used nowadays as they possess unique properties, such as low T_g (-120 °C) [1], high T_d (> 400 °C) and optical transparency [2]. These properties make silicon-based resins good candidates to play the role of protective layers on top of flexible solar cells for space applications as the technique used now (coverglasses on top of the cells) does not allow flexibility [3,4].

Although many efforts were put to protect materials from space environment, most of the researches focused on protection from atomic oxygen (AO) [5–8], electrons [9] and UV radiations [10–14]. As mentioned by Di *et al* [15], only few works were conducted on proton irradiation protection. The best working solutions were nanocomposites with fillers such as detonation nanodiamond [16,17], ZnO [18,19], various metal oxides [20–22], polyoctahedral silsesquioxanes [23] (POSS) or single wall carbon nanotubes (SWCNTs) [24,25].

Looking at space geostationary environment, proton irradiation causes progressive cracking as well as yellowing of PDMS resins [26–29]. Mass loss is also observed due to the outgassing of volatile molecules such as H_2, CH_4, and silanones. Decrease of the amount of Si-C bonds was proven by infrared spectroscopy [26,29] concomitantly with an increase of the Si-O-Si bonds

due to the loss of organic parts such as methyl groups. These observations lead to the conclusion that the surface of the resin changed for a structure close to inorganic silica (SiO_x) [15,29]. It was also observed that this layer does not seem to be further degraded by proton irradiation, leading to the idea of preventing degradation by inserting SiO_2 NPs at the surface of the resin so that the latter would preserve its transparency and flexibility while allowing protons to deliver their energy mainly in radiation-resistant silica. Indeed, it is known that the stopping power of materials depends mainly on their density [30] and calculations made using NIST PSTAR tables [31] showed that a silica layer of about 2.5 µm would have one sufficient to block 240 keV protons.

Following previous unpublished work [33], here is presented the elaboration of class-I and class-II hybrid materials consisting of PDMS resins bearing a layer of non or vinyl-functionalized, compactly assembled SiO_2 NPs at their surface and their effect on the reduction of cracking and yellowing after proton irradiation are presented.

EXPERIMENTAL SECTION

Class-I and class-II hybrid materials were prepared in 3 steps: first SiO_2 NPs were synthesized and functionalized, then they were self-assembled into a photonic crystal and consequently embedded into the PDMS matrix.

Chemicals and Materials.

Poly(dimethylsiloxane) (PDMS) was provided by MAP as a bi-component material: base and hardener. The base contains predominantly vinyl-terminated PDMS and Pt catalyst (Karstedt catalyst). The hardener is a hydride based siloxane. The cross-linked reference PDMS sample was prepared by mixing the base with the hardener in a 10:1 weight ratio. Absolute ethanol (VWR), tetraethyl orthosilicate (TEOS) and L-arginine (both Fluka), vinyltriethoxysilane

(ABCR) as well as ammonium hydroxide (28 % NH_3, Alfa Aesar) were used as received without further purification.

Synthesis and functionalization of SiO_2 NPs.

SiO_2 NPs with controlled shapes and sizes were synthesized following the modified Stöber method. It consists firstly in the synthesis of small irregular SiO_2 NPs called seeds, later undergoing a growth step in a Stöber medium [32].

To synthesize seeds, 100 mL of a 6 mM L-arginine solution were transferred into a 250 mL flask mounted with a condenser and heated at 60 °C. When the temperature was stabilized at 60 °C, 8 mL of TEOS (36.1 mmol) were added to the medium. The mixture was stirred lightly in order to allow the formation of a small vortex, homogenizing the aqueous phase without disturbing the floating organic phase consisting of TEOS. The reaction was left heated and stirred until total consumption of the TEOS (around 2 to 3 days).

To obtain 260 nm nanoparticles from the seeds previously synthesized, 455 mL absolute ethanol (7.79 mol), 35 mL ammonia aqueous solution (0.52 mol) and 250 µL of the seed solution were transferred to a 1L round flask. 35.6 mL of TEOS (160.6 mmol) were added to the mix dropwise thanks to a syringe driver at a volumetric flow rate of 0.5 $mL.h^{-1}$. The concentration of the solution was determined with a dry extract. A few mL of the solution were dialyzed against pure water for DLS experiments.

To functionalize nanoparticles with vinyl moieties, a calculated volume of vinyltriethoxysilane, thanks to Equation 1, was added directly to a known volume of SiO_2 NPs in their Stöber medium. d_{FA} represents the nominal grafting density (nm^{-2}) of the functionalizing agent, M_{FA} its molar mass and ρ_{FA} its density. The mixture was stirred for 3 h at 25 °C before being refluxed for 1 h. The particles were used directly after their concentration was measured with a dry extract.

$$V_{FA} = \frac{6 \cdot d_{FA} \cdot M_{FA} \cdot V_{SiO_2} \cdot C_{SiO_2}}{N_A \cdot \rho_{FA} \cdot \rho_{SiO_2} \cdot D_{SiO_2}} \quad \text{(Eq. 1)}$$

Self-assembly of nanoparticles and creation of a silica layer of controlled thickness.

A volume of 250 nm in diameter SiO_2 NPs solution was transferred to a Petri dish of known radius r. To obtain a silica layer of thickness h, the volume to be transferred to the flask was calculated thanks to the following equation 2:

$$V = \frac{\rho_{SiO_2} \cdot 0.74 \cdot \pi r^2 h}{C_{SiO_2}} \quad \text{(Eq. 2)}$$

Then, the petri dish was transferred to an oven where it was left at 70 °C under vacuum in order to remove the Stöber medium and let the nanoparticles self-assemble. Once out of the oven, the content of the Petri dish appeared green in reflection and pink in transmission as can be seen on Figure 1, due to the self-assembly of the nanoparticles into a photonic crystal [34].

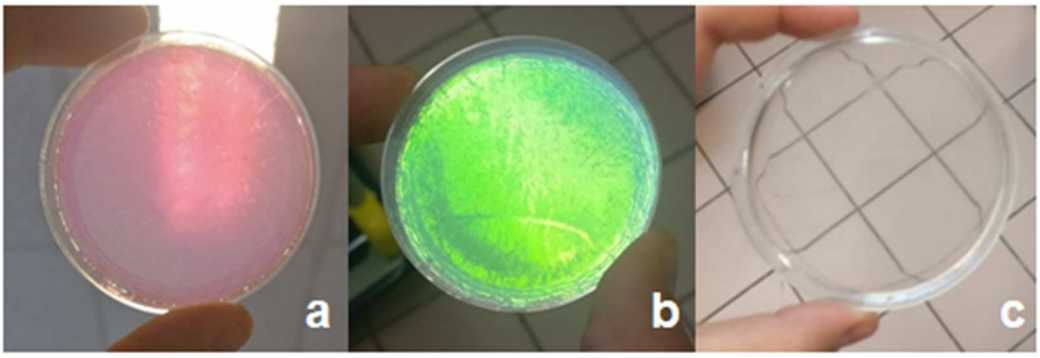

Figure 1: a) self-assembled SiO_2 NPs observed in transmission b) self-assembled SiO_2 NPs observed in reflexion c) same nanoparticles after PDMS was poured over and cross-linked

Embedding of the silica layer in the PDMS resin.

PDMS was found in the form of a base and a hardener to be mixed in a 10:1 weight ratio. As the refractive indexes of silica and PDMS are very close one from the other (respectively 1.475 and [1.42 to 1.46] depending on the considered wavelength) [35,36] the content of the Petri dish slowly turned transparent as the PDMS diffused through interstitial spaces between the nanoparticles. The Petri dish was then transferred to an oven for cross-linking of the resin (15 h at 70 °C). After this step, final materials could simply be peeled off the Petri dish and used as they were following a similar procedure as the one developed by Sun and coworkers [37].

Characterization of materials.

The sizes of the synthesized nanoparticles were analyzed by dynamic light scattering (DLS) at 90° on a Malvern Zetasizer Nano ZS90 apparatus after being dialyzed against milli-Q water. The PDMS matrixes bearing nanoparticles were characterized by UV-vis-NIR spectroscopy on a Perkin Elmer lambda 1050 in transmission mode in a spectral range from 250 to 2500 nm to verify their optical transparency. The spectra were obtained with a scanning speed of 400 nm per minute and at a resolution of 1 nm. Scanning Electron Microscopy experiments were conducted on a Zeiss GeminiSEM300 in high vacuum mode after metallization of the samples with platinum. Optical microscopy was carried out with a Karl Zeiss microscope mounted with a 10 megapixels Canon PowerShot A640 camera. FTIR-ATR spectra were performed on a Bruker VERTEX 70 spectrometer, equipped with diamond crystal (GladiATR PIKE technologies) for attenuated total reflection mode. The spectra were acquired from 4000 to 400 cm^{-1} at room temperature using 64 scans at a resolution of 2 cm^{-1}.

Accelerated ageing of materials.

Proton irradiations were conducted in the MIRAGE facility at ONERA, similar to the SEMIRAMIS one described in the literature [38]. It consists of a high-vacuum chamber coupled with a 2.5 MeV Van de Graff proton accelerator. The vacuum chamber allowed the pressure to

be kept under 10^{-5} mbar. The incoming protons had an energy of 240 keV. The samples were irradiated with a flux of 1.25×10^{11} p^+ cm^{-2} s^{-1} (20 nA cm^{-2}). The total fluence was 3×10^{15} p^+ cm^{-2} for a total surface dose of 2×10^8 Gy. The temperature of the sample holder was maintained at 40 °C for the duration of the test.

RESULTS AND DISCUSSION

Control samples were prepared by mixing the resin's base and hardener in a 10:1 weight ratio and cross-linking them in an oven for 15 h at 70 °C after degassing. SiO_2 NPs were prepared following a two-stage modified Stöber method [39] developed by Désert and coworkers [32]. This method allows the synthesis of monodisperse SiO_2 NPs with controlled size and morphology. This synthesis results in a solution of known concentration of SiO_2 NPs in their Stöber medium. These nanoparticles can be used directly or can be functionalized [40–42] using vinyltriethoxysilane in order to graft vinyl moieties at the surface of the nanoparticles. Nanoparticles with diameters ranging from 50 to 260 nm and nominal grafting densities ranging from 0 to 10 functions per square nanometers were prepared and used directly in their Stöber medium (Supporting Information, Schemes S1 and S2).

In order to first evaluate the impact of the SiO_2 NPs layers' thicknesses on the stability of the materials, class-I hybrid materials consisting of a layer of controlled thickness of non-grafted SiO_2 NPs arranged in a compact manner and embedded at the surface of a PDMS matrix were synthesized. Materials with 260 nm diameter nanoparticles with layer thicknesses equal to 1, 3, 7, 14 and 28 µm were prepared (Supporting Information, Table S1).

In order now to evaluate the impact of the grafting density of vinyl moieties on SiO_2 NPs, class-II hybrid materials consisting of a layer of controlled thickness of vinyl-decorated SiO_2 NPs arranged in a compact manner and embedded at the surface of a PDMS matrix were synthesized. These nanoparticles are bonded to the polymer matrix through covalent linking assured by

hydrosilylation in the presence of a Karstedt catalyst (Pt^0) [43] already existing in the formulation of the resin's base. Due to the heightened sensibility of the synthesis of SiO_2 NPs to parameters, such as temperature or concentrations, materials with two different diameters nanoparticles (250 and 260 nm) with a layer thickness of 7 µm and with different nominal grafting densities ranging from 0.01 to 10 vinyl functions per square nanometers were prepared (Supporting Information, Table S2).

Finally, to evaluate the impact of the size of the SiO_2 NPs, class-II hybrid materials were synthesized. These nanoparticles are bound to the polymer matrix through covalent linking assured by the Karstedt catalyst present in the resin's base. Materials with 50, 100 and 260 nm diameter nanoparticles with a layer thickness of 7 µm and with different nominal grafting densities were prepared (Supporting Information, Table S3). The grafting densities on the different nanoparticles were chosen so that the amount of vinyl moieties per unit of volume was equivalent to the ones on 260 nm nanoparticles with grafting densities of 0.1 and 1 vinyl.nm^{-2}.

Pre-irradiation UV-vis-NIR characterization

The spectra of all the materials synthesized in the full 250 – 2500 nm range are available in the electronic supporting information (Supporting Information, Figure S1). The effect of the silica layers' thicknesses on the materials' transparency was investigated using non-functionalized 260 nm in diameter silica. The spectrograms of these materials in the range 250 – 750 nm are presented on Figure 2. Samples are named as follow: diameterOfNanoparticles_graftingDensity_thicknessOfSilicaLayer_sampleNumber.

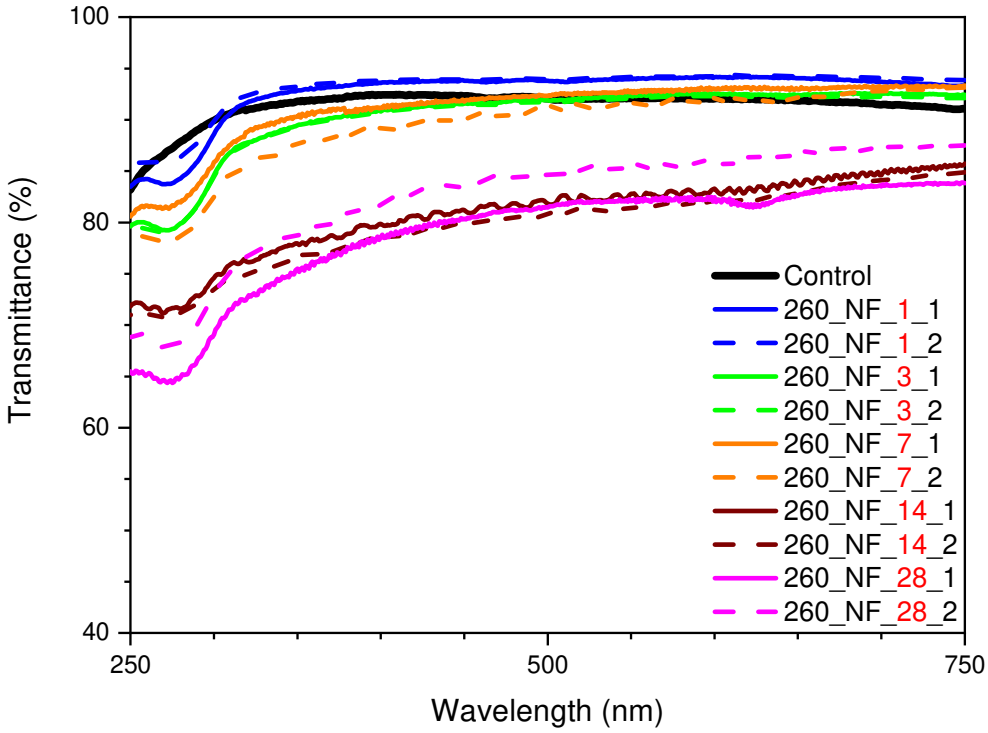

Figure 2: UV-vis spectra of materials containing non-functionalized nanoparticles with different layer thicknesses before proton irradiation

The materials' transparency is preserved with respect to the pristine resin as long as the SiO_2 NPs layer's thickness does not exceed 7 µm. Below this value, materials keep a transparency equivalent to the one of the plain PDMS resin. This is supposed to be due to the low amount of interfaces that photons have to go through before reaching detectors in the spectrometer, interfaces on which scattering phenomena occur. A noticeable drop in transmittance in the range 250 – 300 nm is observed for all materials containing nanoparticles and is because the nanoparticles are forming a photonic crystal with a characteristic distance of 260 nm, susceptible to interact with incoming photons.

Similarly, UV-vis-NIR experiments were carried out on the synthetized materials in order to evaluate the effect of the grafting density on the transparency of the materials. For this purpose, materials consisting of a PDMS matrix in which is embedded a layer of constant thickness (7

µm) of SiO_2 NPs decorated with vinyl moieties and nominal grafting densities ranging from 0.01 to 10 functions per square nanometers were synthesized. Spectra in the range 250 – 750 nm are shown in Figure 3.

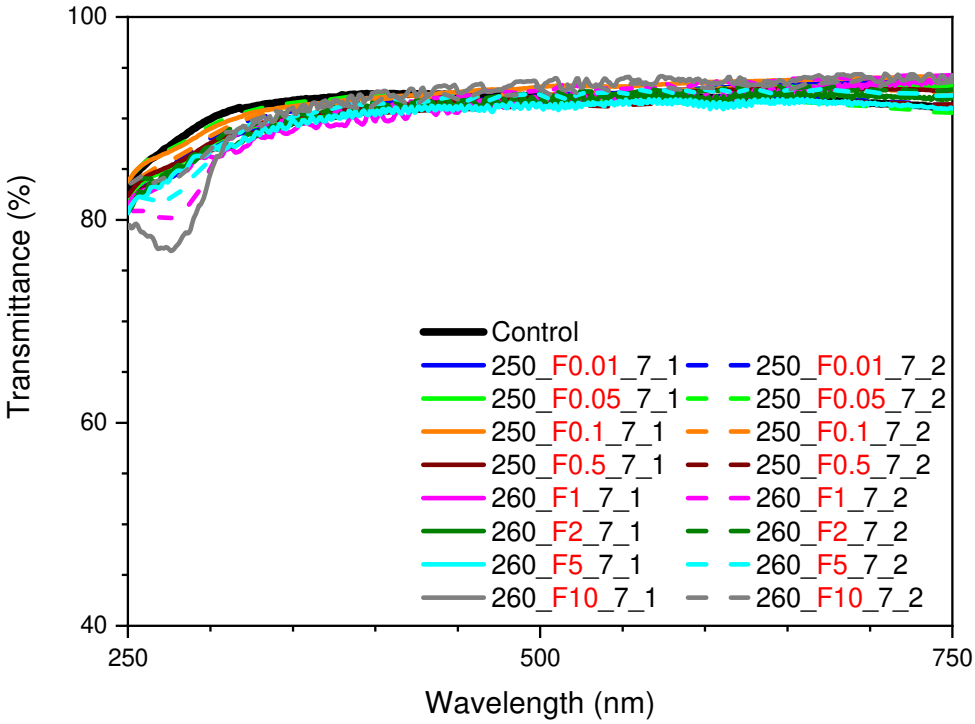

Figure 3: UV-vis spectra of materials containing functionalized nanoparticles at different grafting densities before proton irradiation

No discernable effect of the grafting density on the transparency of the materials was observed. Nonetheless, the effect of the size of the nanoparticles can be observed as the transmittance of the materials containing 260 nm SiO_2 NPs slightly lowers in the range 250 – 300 nm.

Once again, UV-vis-NIR experiments were carried out on the synthetized materials in order to evaluate the effect of the size of the decorated nanoparticles on the transparency of the materials. For this purpose, materials consisting of a PDMS matrix in which is embedded a layer of constant thickness (7 µm) of SiO_2 NPs of decreasing sizes (260 to 50 nm) and decorated with vinyl moieties (Supporting Information, Table S3). Spectra in the range 250 – 750 nm are

available (Supporting Information, Figure S2). A drop in transmittance is observed with decreasing nanoparticles size due to the increased amount of interfaces encountered by light. One can notice as well that the transmittance of materials containing 260 nm SiO_2 NPs slightly lowers in the range 250 – 300 nm for the same reasons above described.

Post-irradiation characterizations

Cracking evaluation

Samples were irradiated in the MIRAGE chamber consisting of a 2.5 MeV Van de Graff proton accelerator linked to a vacuum chamber. Following the irradiation, materials were observed with the naked eye as can be seen on Figure 4.

Figure 4: Naked eye observation of irradiated materials.

On the one hand, materials containing non-functionalized nanoparticles do not seem to have a great stabilizing effect even though they did crack a bit less than control materials. On the other hand, it appears that materials containing functionalized nanoparticles show a significantly reduced amount of cracks though this phenomenon is hard to quantify. Further investigation

led to look at every sample with an optical microscope. The images obtained are presented Figure 5.

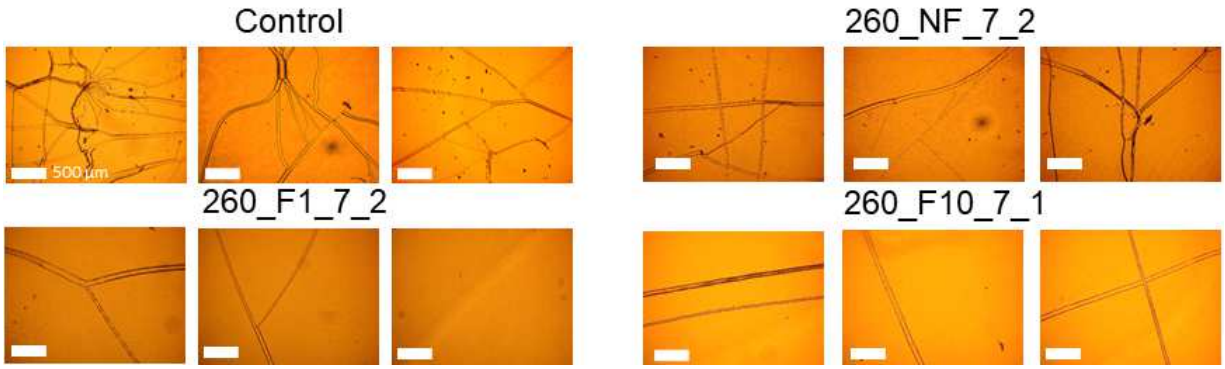

Figure 5: Images of irradiated materials obtained by optical microscopy (x50). The scale bar is the same for every sample (500 µm). Yellowing due to microscope lamp

Once again, it appears that the amount of cracks per unit area is lowered on stabilized materials though this factor is hard to evaluate quantitatively. There is a direct link between the amount of cracks and the thermo-optical properties of the materials as cracks lead to scattering phenomena partly responsible for the drop in transmittance observed after proton irradiation. Scanning electron microscopy characterizations were also performed to bring evidence about a few assumptions made during the elaboration of the samples. Images demonstrating the robustness of the self-assembly method can be seen Figure 6.

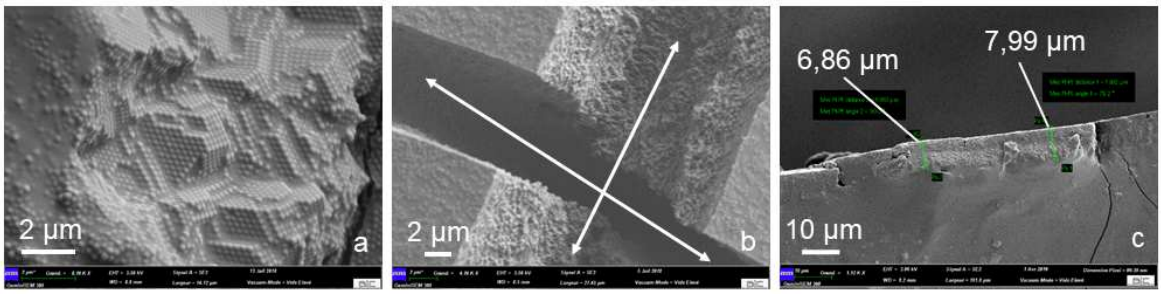

Figure 6: a) Side view of a teared sample b) intersection of two cracks on an irradiated material c) Side view of a 7 µm thick silica layer embedded in the resin

Figure 6.a shows the nanoparticles are close-packed forming a photonic crystal and justifies the use of the factor 0.74 (which is the packing fraction of a dense packing of spheres) in (Eq. 2) allowing calculation of the volume of SiO_2 NPs solution required to create a layer of nanoparticles of controlled thickness. This explains as well the optical properties of the silica layer before embedding in the resin. On Figure 6.b is shown the intersection of two cracks on an irradiated material containing undecorated nanoparticles. It shows that the particles are well coated with PDMS suggesting a good wetting. Figure 6.c shows measurement carried out on a non-irradiated material demonstrating that the actual thickness of the silica layer is in accordance with the theoretical one.

Post-irradiation UV-Vis-NIR characterization

The same UV-vis-NIR experiments as the ones carried out before irradiation were conducted again to evaluate the stabilizing effect of the SiO_2 NPs layer regarding the transparency of the materials. The spectra in the full 250 – 2500 nm range for all tested materials are available (Supporting Information, Figure S3). Spectra of the same materials used for Figures S2, 2 and 3 after proton irradiation are also available (Figure 7 and Supporting Information, Figures S4, and S5). What was true before irradiation remains: if the layer is too thick, the transmittance drops. Materials containing nanoparticles with layer thickness greater than 7 µm were stabilized in the UV range (up to 350 nm) whereas they are detrimental to transparency in the visible range: non-functionalized nanoparticles do not offer great stabilization of the resin.

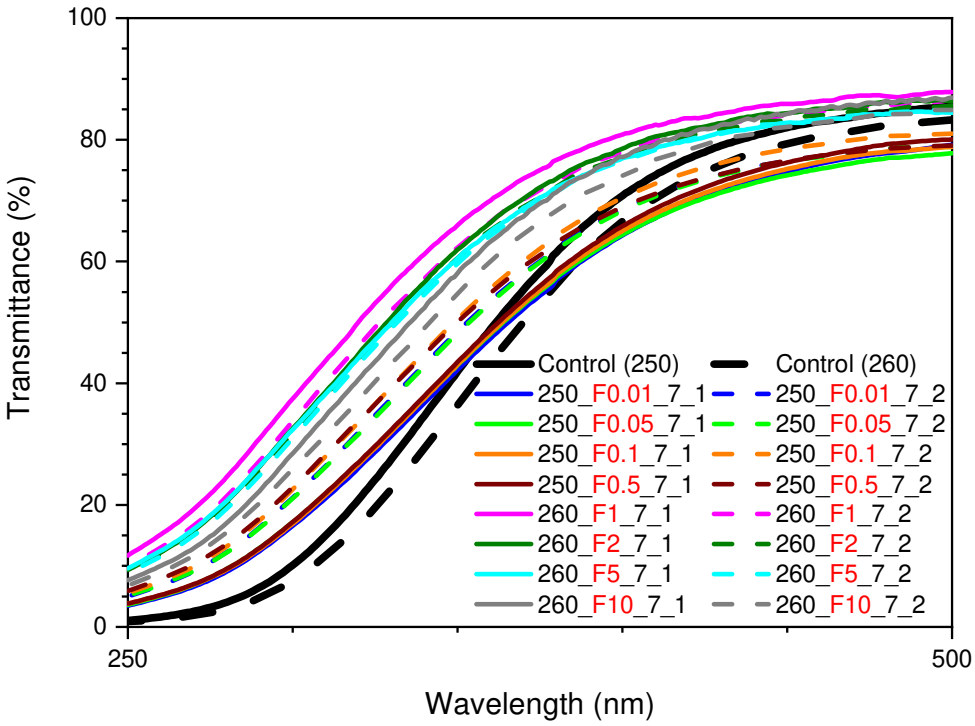

Figure 7: UV-vis spectra of materials containing functionalized nanoparticles at different grafting densities after proton irradiation

Concerning the effect of the grafting density, spectra show that every material containing functionalized nanoparticles was stabilized in the UV region in comparison with control samples. Besides, an effect of the grafting density was shown. It appears that there is a maximum in terms of stabilization when nanoparticles are functionalized at a nominal grafting density of 1 vinyl.nm^{-2}. We believe that these materials offer sufficient cohesion between the SiO_2 NPs, while preserving flexibility necessary to allow constraint relaxation due to the densification of the matrix. These materials are therefore less subject to cracking, thus leading to less scattering than other materials containing SiO_2 NPs grafted with higher vinyl contents. The impact of the size of the nanoparticles was also investigated. Once again, the conclusions that could be drawn from the pre-irradiation characterization are still valid: materials containing smaller nanoparticles offer more interfaces per unit of distance leading to more scattering

events, eventually bringing down transmittance. Materials that had the best stabilizing effect were those containing 260 nm SiO_2 NPs. As the transparency range of interest is 250 – 2500 nm for spatial applications, one can say that the optimal size for nanoparticles is 250 nm. Indeed, even if it seems here that 260 nm nanoparticles offer greater stabilization, one should remember that in terms of original transparency, that is to say before irradiation, 260 nm nanoparticles interact with light therefore bringing down transmittance in the 250 – 300 nm region. That is why it can confidently be said that the most suitable material would be one containing 250 nm nanoparticles decorated with vinyl moieties at a nominal grafting density of 1 function per square nanometer.

In order to quantify the stabilization in terms of transparency of the resin, the solar absorptances (α_S) of the materials were calculated before and after irradiation according to Equation 3 [44].

$$\alpha_S = \frac{\int_{250}^{2500} A(\lambda) I_S(\lambda) d\lambda}{\int_{250}^{2500} I_S(\lambda) d\lambda} \quad \text{(Eq.3)}$$

The solar absorptance corresponds to the effectiveness of a material in absorbing radiant energy emitted by the sun. In the case presented here, α_S should be as small as possible, this would be interpreted as a proof of transparency in the wavelength range of interest. Indeed, these materials should be as transparent as possible in the region of the spectrum where the sun deliver maximum power while it would not be as much of a problem elsewhere in the said spectrum.
$I_S(\lambda)$ is tabulated in norm ASTM E 490 and corresponds to the energy carried by photons emitted by the sun per unit of time per unit of area for a given wavelength ($mW.cm^{-2}.nm^{-1}$). Besides, $A(\lambda)$ –the spectral absorptance of the material– is equal to $1 - (R(\lambda) + T(\lambda))$. It was decided to calculate the spectral absorptances of the materials considering $R(\lambda) = 0$ as a decent approximation. Indeed, the aim here was not to obtain true values of solar absorptivity but to be able to compare different materials. Due to the size of the sample holder in the MIRAGE

facility, two different batches had to be irradiated separately. To reach better comparability of the different batches, each material was compared to the control sample that was irradiated in the same time as itself. Results are gathered in Table 1 and 2 relating respectively to batches 1 and 2.

Table 1: Comparison of the solar absorptances of synthesized materials (batch 1), before and after proton irradiation.

Sample name	α_S before irradiation*	α_S after irradiation*	Rate of change (%)	$\Delta(\alpha_S)$*	Rate of change in $\Delta(\alpha_S)$ compared to control sample (%)
Control sample	0.10	0.21	124	0.12	N/A
260_F1_7_1	0.09	0.14	56.5	0.05	-56.1
260_F1_7_2	0.08	0.15	89	0.07	-39.4
260_F2_7_1	0.09	0.16	68.5	0.06	-45.0
260_F2_7_2	0.09	0.16	86	0.07	-36.8
260_F5_7_1	0.10	0.17	66.5	0.07	-43.0
260_F5_7_2	0.09	0.17	91.5	0.08	-31.0
260_F10_7_1	0.08	0.16	104	0.08	-32.2
260_F10_7_2	0.08	0.17	106	0.09	-24.8
260_NF_1_1	0.08	0.20	161.5	0.12	2.9
260_NF_1_2	0.07	0.19	157.5	0.11	-3.7
260_NF_3_1	0.09	0.20	123	0.11	-6.6
260_NF_3_2	0.10	0.22	129.5	0.12	5.3
260_NF_7_1	0.09	0.17	94.5	0.08	-28.6
260_NF_7_2	0.09	0.21	131.5	0.12	2.3
260_NF_14_1	0.16	0.28	74.5	0.12	2.8
260_NF_14_2	0.17	0.25	52.5	0.09	-26.5
260_NF_28_1	0.18	0.36	100	0.18	52.0
260_NF_28_2	0.15	0.32	112.5	0.17	44.8

*alpha values were rounded for readability

Table 2: Comparison of the solar absorptances of synthesized materials (batch 2), before and after proton irradiation.

Sample name	αs before irradiation*	αs after irradiation*	Rate of change (%)	Δ(αs)*	Rate of change in Δ(αs) compared to control sample (%)
Control sample	0.09	0.27	209	0.18	N/A
250_F0.01_7_1	0.08	0.22	156	0.13	-28.5
250_F0.01_7_2	0.09	0.23	140	0.13	-28.5
250_F0.05_7_1	0.09	0.23	163.5	0.14	-24
250_F0.05_7_2	0.09	0.22	133	0.12	-32.5
250_F0.1_7_1	0.08	0.22	177	0.14	-25
250_F0.1_7_2	0.09	0.20	134.5	0.12	-37.5
250_F0.5_7_1	0.10	0.20	110	0.10	-43
250_F0.5_7_2	0.09	0.22	153.5	0.13	-28.5
100_F0.39_7_1	0.09	0.24	151	0.14	-23
100_F0.39_7_2	0.09	0.33	248	0.23	27
100_F0.039_7_1	0.10	0.29	188	0.19	2.72
100_F0.039_7_2	0.09	0.23	168.5	0.14	-22
50_F0.19_7_1	0.10	0.30	202.5	0.20	11
50_F0.19_7_2	0.11	0.30	161.5	0.18	-1
50_F0.019_7_1	0.12	0.32	176.5	0.20	10.5
50_F0.019_7_2	0.15	0.36	142	0.21	15.5

*alpha values were rounded for readability

The rates of change were calculated as follow: $Rate\ of\ change = \frac{\alpha_S(before)-\alpha_S(after)}{\alpha_S(before)} * 100$ (Eq.4). These values, as well as the solar absorptances differentials, give a good idea of how much the transparencies of the materials have evolved from their initial states to their aged ones. Solar absorptances differentials are not sufficient to allow ageing comparisons between different batches for reasons aforementioned. In order to compare the two batches, solar absorptances differential must be normalized by the $\Delta(\alpha_S)$ value of the control sample. This is why the rates of change in solar absorptances differentials ($R\%\Delta(\alpha_S)$) compared to control

samples were calculated following Equation 5: the smaller this value; the better the stabilization of the material in terms of transparency. It has to be noted that a material with a small solar absorptance differential may seem like an interesting one even though it could have a terrible initial transparency, incompatible with its usage: this is why one has to look upon the initial solar absorptances. Fortunately, every material presented here presents at least a decent initial absorptance so that the rate of change in solar absorptances differential will be the only factor discussed from now on.

$$\text{Rate of change in solar absorptances differential } [R\%\Delta(\alpha_S)] = \frac{\Delta(\alpha_S)\text{sample} - \Delta(\alpha_S)\text{control}}{\Delta(\alpha_S)\text{control}} * 100$$

(Eq.5)

$R\%\Delta(\alpha_S)$ values could be as high as 52 % for a sample containing a 28 µm thick layer of 260 nm non-functionalized nanoparticles, meaning that this material aged even worse than its control in terms of transparency. This is also the case for the great majority of materials containing non-functionalized nanoparticles or smaller ones, though the values obtained were more lenient. It was even found that some of these materials could be stabilized compared to control samples as some of the values obtained were negative, e.g. for 100_F0.39_7_1 or 100_F0.039_7_2 with values of -23 % and -22 %, respectively. Non-functionalized nanoparticles (NF_7_1 and NF_7_2) may have a positive effect on the stabilization of the optical properties of the materials in which they were embedded, though this effect was not repeatable from one sample to another (with values of $R\%\Delta(\alpha_S)$ of -28.6 % and 2.3 %, respectively). Indeed, the cohesion of the nanoparticles with the matrix relying only hydrogen bonds and weak interactions is not sufficient to disable cracking, leading to scattering phenomena. Materials containing functionalized nanoparticles were all stabilized compared to control samples as long as the thickness of the silica layer was in the range 3 – 14 µm. Indeed, for these materials, $R\%\Delta(\alpha_S)$ were all negatives ranging from -24 % for 250_F0.05_7_1 to -

56.1 % for 260_F1_7_1. Altogether, R%Δ(α_S) values ranged from -56.1 % to 52 % and are both comparable and representative of the materials' ageing. The stabilization previously observed qualitatively on the raw spectra concerning the grafting density of the nanoparticles is now characterized quantitatively.

Materials containing 7 µm thick, 260 nm functionalized SiO_2 NPs were all stabilized regardless of the grafting density on the NPs with rates of change in solar absorptances differential starting at least at -25 %. Besides, there is a clear trend showing that the stabilizing effect shown with functionalized 250-260 nm nanoparticles assembled into a 7 µm thick layer reaches a maximum when the nominal grafting density of vinyl moieties is around 1 function per square nanometer as foreseen during the post-irradiation spectroscopic characterization (Figure 8). Materials containing a 7 µm thick, 260 nm SiO_2 NPs functionalized with a nominal grafting density of 1 vinyl/nm² were the most stabilized as their rate of change in solar absorptivity compared to the control samples was ranging from almost -40 to -55 %.

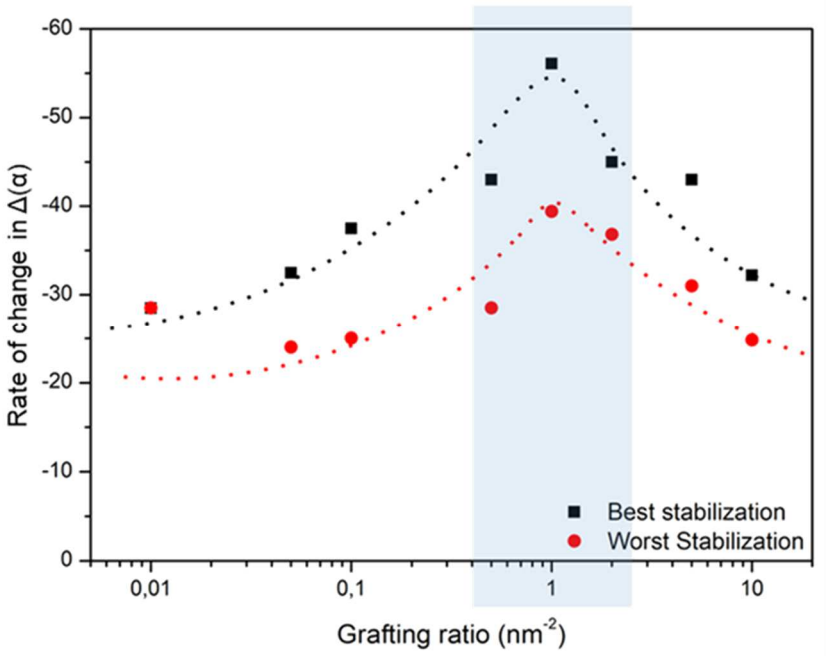

Figure 8: effect of the grafting density on the optical stabilization of samples containing nanoparticles of around 250 nm and assembled into a 7 µm thick layer

FTIR-ATR study of degradation and stabilization mechanisms

Materials containing nanoparticles, whether functionalized or not, were stabilized in comparison with unprotected ones; better understanding of the underlying mechanisms was needed. Materials were then studied by means of FTIR-ATR both before and after irradiation. Spectra of control material and 260_F1_7_1 both before and after irradiation are presented Figures 9 and 10.

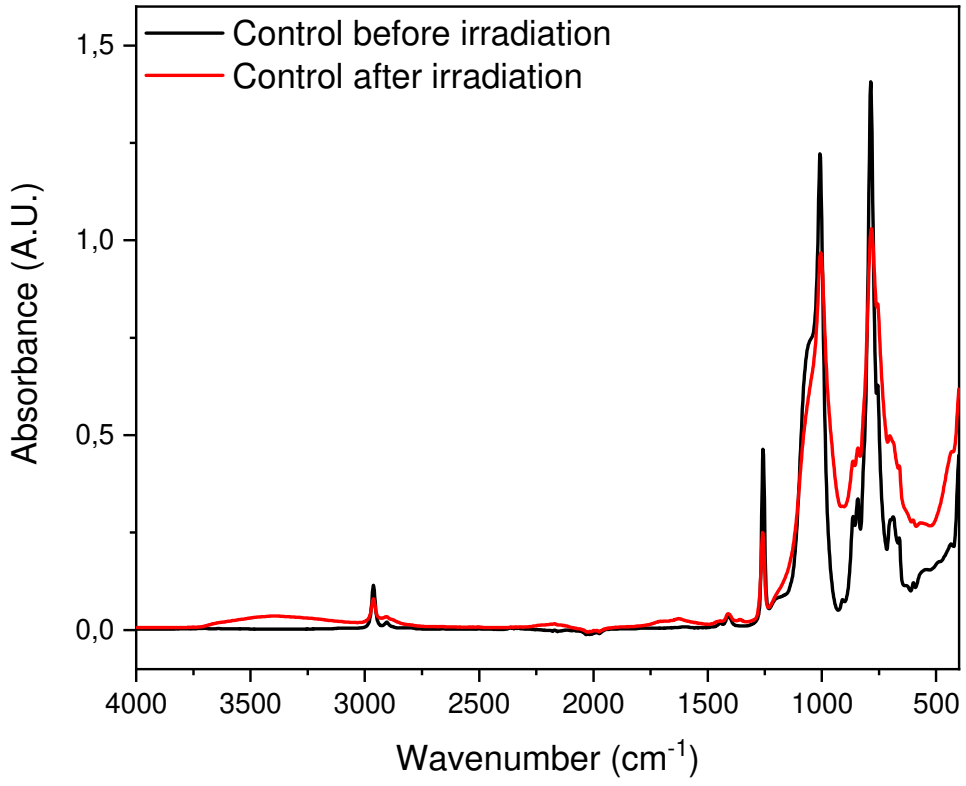

Figure 9: FTIR-ATR spectra of a control sample before and after proton irradiation

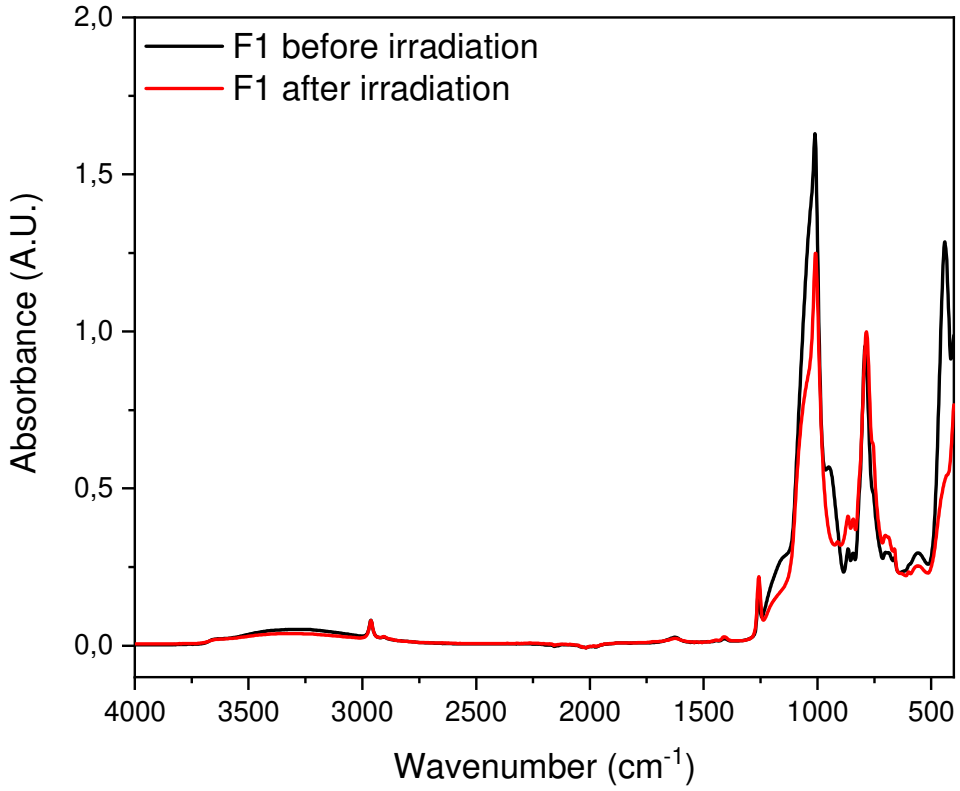

Figure 10: FTIR-ATR spectra of 260_F1_7_1 sample before and after proton irradiation

The most intense bands are the $–CH_3$ asymmetric rocking and Si-C asymmetric stretching at 790 cm^{-1}, and both the Si-O-Si symmetric and asymmetric stretching at respectively 1010 and 1060 cm^{-1} followed by symmetric $–CH_3$ bend at 1258 cm^{-1}. The intensities of these bands decrease in all cases, showing backbone degradation (chain scissions) as well as modification of the pendant methyl groups. This is consistent with the literature about the degradation of PDMS under proton irradiation [26-29]. Nonetheless, the degradations occurring on the organic part of the polymer are much more pronounced in the unprotected samples (especially at 1258 and 790 cm^{-1}). The same conclusion can be drawn from the bands at 2904 and 2960 cm^{-1}, attributed to asymmetric stretching of $–CH_3$ in $Si-CH_3$. This shows that though composites are degraded as well, the density of the degradations is lowered compared to unprotected materials.

Concerning the densification of the matrix, ATR-IR spectroscopy was carried out on vinyl-functionalized nanoparticles as it can be hard to distinguish Si-O vibration bands due to PDMS from the one due to silica-like materials. These nanoparticles do not contain any PDMS, thus all the bands (except the ones related to the vinyl moieties) appearing on the spectrum are the signature of silica nanoparticles. On Figure S10 can be seen superposition of 3 spectra: control sample both before and after irradiation and silica nanoparticles. It is striking to see that the main modifications in the spectra from before to after irradiation can be attributed to the formation of silica. Indeed, new band appears on unprotected materials at around 3400 cm^{-1}, corresponding to the formation of –OH bonds after scission of the polymer backbone and formation of the silica like layer as described in the literature [26]. The same conclusion can be drawn from the bands at 1120 – 1240, 860 – 985, and 430 – 500 cm^{-1}, increasing in all cases in the plain PDMS resin from before to after irradiation and being typical of silica nanoparticles as can be seen from their ATR-IR spectrum. Further proof of the densification of the matrix under proton irradiation is also described in the article cited above.

Concerning the yellowing of the resin, considered in the literature to originate from the formation of carbonyl moieties [26,45], it appears that materials containing nanoparticles present a lesser increased absorption band at 1720 cm^{-1} as can be seen of Figure 11. Once again, this is thought to originate from the fact that less organic part is to be degraded in materials containing nanoparticles versus those containing none. Composite materials made of PDMS resin bearing nanoparticles at their surface are more resistant to proton irradiation, not because they disable the classical mechanisms of degradation described in the literature but because they reduce the amount of organic matter to be degraded, thus limiting the formation of new undesired moieties.

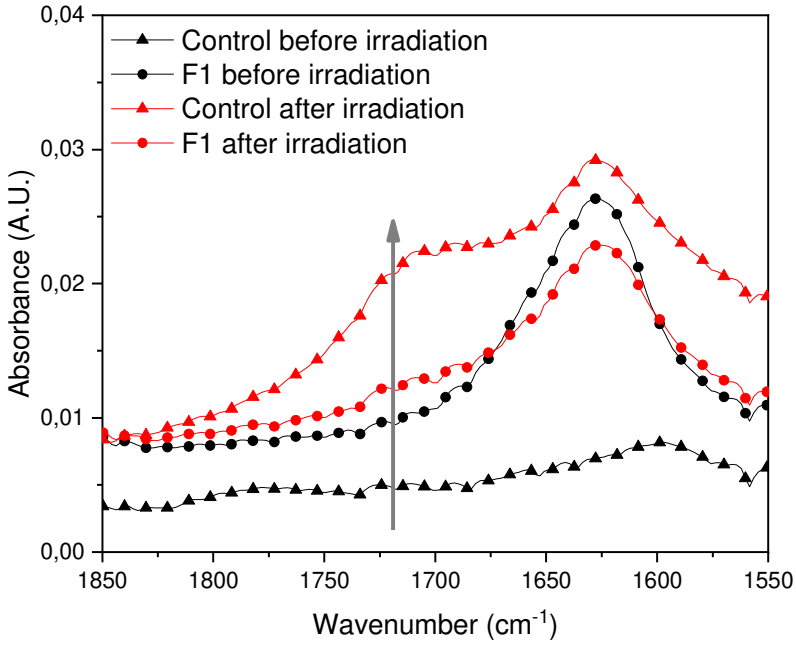

Figure 11: FTIR-ATR spectra of control and 260_F1_7_1 samples in the 1850-1550 cm^{-1} region

CONCLUSIONS

Class-I and class-II hybrid materials were elaborated embedding 50 to 260 nm diameter SiO_2 NPs at the surface of a PDMS matrix. SiO_2 NPs used for the class-II materials were functionalized with vinyl moieties at different nominal grafting densities ranging from 0.01 to 10 functions per square nanometer. It was shown by UV-vis-NIR spectroscopy that the transparency of the resin in the entire 250 – 2500 nm range was not modified by the addition of the nanoparticles as long as the thickness of the silica layer was not exceeding 7 µm, regardless of the functionalization of the nanoparticles. After proton irradiation in high vacuum, samples were analyzed again by means of UV-vis-NIR. Data from spectroscopy allowed solar absorptivities of the samples to be calculated. It was shown that non-functionalized particles were not a very good mean of protection as the optical properties of materials containing them

were only slightly improved compared to the ones of control samples. Besides, after optical and electronic microscopy, it appeared that these materials still cracked upon proton irradiation. Nonetheless, materials containing vinyl-functionalized nanoparticles were greatly stabilized as their rates of change in solar absorptances compared to control samples were up to 50 %. Furthermore, these materials shown a greater capacity to resist cracking as can be seen with the naked eye as well as with optical microscopy. The study of the samples by means of FTIR-ATR showed that the stabilization of the materials originates from the fact that protected materials offer less organic matter to be degraded. These materials appear to be a promising way of protecting flexible solar panels in regards to proton irradiation in spatial environment.

AKNOWLEDMENTS

The authors would like to thank Claude Pons and Romain Rey from ONERA Toulouse Center for running proton irradiation experiments.

REFERENCES

[1] Fragiadakis, D.; Pissis, P.; Bokobza, L. Glass Transition and Molecular Dynamics in Poly(Dimethylsiloxane)/Silica Nanocomposites. *Polymer* **2005**, *46* (16), 6001–6008.

[2] Roychowdhury, T.; Cushman, C. V.; Synowicki, R. A.; Linford, M. R. Polydimethylsiloxane: Optical Properties from 191 to 1688 Nm (0.735–6.491 EV) of the Liquid Material by Spectroscopic Ellipsometry. *Surface Science Spectra* **2018**, *25* (2), 026001.

[3] Wilt, D.; Snyder, N.; Jenkins, P.; Gray, A. Novel Flexible Solar Cell Coverglass for Space Photovoltaic Devices. *2013 IEEE 39th Photovoltaic Specialists Conference (PVSC)* **2013**.

[4] Smeenk, N.; Mooney, C.; Feenstra, J.; Mulder, P.; Rohr, T.; Semprimoschnig, C.; Vlieg, E.; Schermer, J. Space Environmental Testing of Flexible Coverglass Alternatives Based on Siloxanes. *Polymer Degradation and Stability* **2013**, *98* (12), 2503–2511.

[5] Minton, T. K.; Wright, M. E.; Tomczak, S. J.; Marquez, S. A.; Shen, L.; Brunsvold, A. L.; Cooper, R.; Zhang, J.; Vij, V.; Guenthner, A. J.; Petteys, B. J. Atomic Oxygen Effects on POSS Polyimides in Low Earth Orbit. *ACS Applied Materials & Interfaces* **2012**, *4* (2), 492–502.

[6] Duo, S.; Chang, Y.; Liu, T.; Zhang, H. Atomic Oxygen Erosion Resistance of Polysiloxane/POSS Hybrid Coatings on Kapton. *Physics Procedia* **2013**, *50*, 337–342.

[7] Duo, S. W.; Song, M. M.; Li, T. Z.; Luo, Y.; Li, M. S. Polyhedral Oligomeric Silsesquioxane/PDMS Hybrid Coating Protecting Polyimide from Atomic Oxygen Erosion. *Advanced Materials Research* **2011**, *189-193*, 336–339.

[8] Duo, S.; Li, M.; Zhu, M.; Zhou, Y. Polydimethylsiloxane/Silica Hybrid Coatings Protecting Kapton from Atomic Oxygen Attack. *Materials Chemistry and Physics* **2008**, *112* (3), 1093–1098.
[9] Stevenson, I.; David, L.; Gauthier, C.; Arambourg, L.; Davenas, J.; Vigier, G. Influence of SiO2 Fillers on the Irradiation Ageing of Silicone Rubbers. *Polymer* **2001**, *42* (22), 9287–9292.
[10] Chiavari, C.; Balbo, A.; Bernardi, E.; Martini, C.; Zanotto, F.; Vassura, I.; Bignozzi, M.; Monticelli, C. Organosilane Coatings Applied on Bronze: Influence of UV Radiation and Thermal Cycles on the Protectiveness. *Progress in Organic Coatings* **2015**, *82*, 91–100.
[11] Planes, M.; Coz, C. L.; Soum, A.; Carlotti, S.; Rejsek-Riba, V.; Lewandowski, S.; Remaury, S.; Solé, S. Polydimethylsiloxane/Additive Systems for Thermal and Ultraviolet Stability in Geostationary Environment. *Journal of Spacecraft and Rockets* **2016**, *53* (6), 1128–1133.
[12] Girigoswami, K.; Viswanathan, M.; Murugesan, R.; Girigoswami, A. Studies on Polymer-Coated Zinc Oxide Nanoparticles: UV-Blocking Efficacy and in Vivo Toxicity. *Materials Science and Engineering: C* **2015**, *56*, 501–510.
[13] Lima, J. F. D.; Martins, R. F.; Serra, O. A. Transparent UV-Absorbers Thin Films of Zinc Oxide: Ceria System Synthesized via Sol–Gel Process. *Optical Materials* **2012**, *35* (1), 56–60.
[14] Planes, M.; Brand, J.; Lewandowski, S.; Remaury, S.; Solé, S.; Coz, C. L.; Carlotti, S.; Sèbe, G. Improvement of the Thermal and Optical Performances of Protective Polydimethylsiloxane Space Coatings with Cellulose Nanocrystal Additives. *ACS Applied Materials & Interfaces* **2016**, *8* (41), 28030–28039.
[15] Di, M.; He, S.; Li, R.; Yang, D. Radiation Effect of 150keV Protons on Methyl Silicone Rubber Reinforced with MQ Silicone Resin. *Nuclear Instruments and Methods in Physics Research Section B: Beam Interactions with Materials and Atoms* **2006**, *248* (1), 31–36.
[16] Borjanović, V.; Bistričić, L.; Mikac, L.; Mcguire, G. E.; Zamboni, I.; Jakšić, M.; Shenderova, O. Polymer Nanocomposites with Improved Resistance to Ionizing Radiation. *Journal of Vacuum Science & Technology B, Nanotechnology and Microelectronics: Materials, Processing, Measurement, and Phenomena* **2012**, *30* (4), 041803.
[17] Borjanović V.; Bistričić L.; Vlasov, I.; Furić K.; Zamboni, I.; Jakšić M.; Shenderova, O. Influence of Proton Irradiation on the Structure and Stability of Poly(Dimethylsiloxane) and Poly(Dimethylsiloxane)-Nanodiamond Composite. *Journal of Vacuum Science & Technology B: Microelectronics and Nanometer Structures* **2009**, *27* (6), 2396.
[18] Bistričić, L.; Borjanović, V.; Zamboni, I.; Jakšić, M.; Mcguire, G. E. Spectroscopic Study of Poly(Dimethylsiloxane) ZnO Nanocomposites Exposed to Proton Irradiation. *Macromolecular Symposia* **2014**, *339* (1), 91–99.
[19] Xiao, H.; Li, C.; Sun, M.; Yang, D.; Di, M.; He, S. An Analysis on Optical Degradation of ZnO/Silicone White Paint under Proton Exposure. *Nuclear Instruments and Methods in Physics Research Section B: Beam Interactions with Materials and Atoms* **2008**, *266* (1), 86–92.
[20] Mikhailov, M.; Neshchimenko, V.; Grigorevskiy, A.; Sokolovskiy, A.; Bakhtaulova, A.; Vaschenkov, I. Radiation Stability of Silicon-Organic Varnish Modified with Nanoparticles. *Polymer Degradation and Stability* **2018**, *153*, 185–191.
[21] Mikhailov, M. M.; Neshchimenko, V. V.; Grigorevskii, A. V.; Bakhtaulova, A. S.; Vashchenkov, I. S. Radiation Resistance of Nanomodified Organosilicic Enamel. *Russian Physics Journal* **2018**, *61* (8), 1529–1535.

[22] Li, C.; Neshchimenko, V. V.; Mikhailov, M. M. The Effect of Small Concentrations of Nanopowders on the Radiation Stability of Lacquers. *Astrophysics and Space Science Proceedings Protection of Materials and Structures from the Space Environment* **2017**, 131–138.
[23] Lei, X.-F.; Qiao, M.-T.; Tian, L.-D.; Yao, P.; Ma, Y.; Zhang, H.-P.; Zhang, Q.-Y. Improved Space Survivability of Polyhedral Oligomeric Silsesquioxane (POSS) Polyimides Fabricated via Novel POSS-Diamine. *Corrosion Science* **2015**, *90*, 223–238.
[24] Li, Z.; Nambiar, S.; Zheng, W.; Yeow, J. PDMS/Single-Walled Carbon Nanotube Composite for Proton Radiation Shielding in Space Applications. *Materials Letters* **2013**, *108*, 79–83.
[25] Pulikkathara, M. X.; Shofner, M. L.; Wilkins, R. T.; Vera, J. G.; Barrera, E. V.; Rodríguez-Macías, F. J.; Vaidyanathan, R. K.; Green, C. E.; Condon, C. G. Fluorinated Single Wall Nanotube/Polyethylene Composites for Multifunctional Radiation Protection. *MRS Proceedings* **2002**, *740*.
[26] Huszank, R.; Szilasi, S. Z.; Szikra, D. Ion-Energy Dependency in Proton Irradiation Induced Chemical Processes of Poly(Dimethylsiloxane). *The Journal of Physical Chemistry C* **2013**, *117* (49), 25884–25889.
[27] Zhang, L.; He, S.; Xu, Z.; Wei, Q. Damage Effects and Mechanisms of Proton Irradiation on Methyl Silicone Rubber. *Materials Chemistry and Physics* **2004**, *83* (2-3), 255–259.
[28] Zhang, L.; Xu, Z.; Wei, Q.; He, S. Effect of 200keV Proton Irradiation on the Properties of Methyl Silicone Rubber. *Radiation Physics and Chemistry* **2006**, *75* (2), 350–355.
[29] Szilasi, S. Z.; Kokavecz, J.; Huszank, R.; Rajta, I. Compaction of Poly(Dimethylsiloxane) (PDMS) Due to Proton Beam Irradiation. *Applied Surface Science* **2011**, *257* (10), 4612–4615.
[30] Bromley, D. A. *Treatise on heavy-ion science: Volume 6: Astrophysics, Chemistry, and Condensed Matter*; Springer: Boston, **1985**.
[31] Seltzer, S. Stopping-Powers and Range Tables for Electrons, Protons, and Helium Ions, *NIST Standard Reference Database 124*, National Institute of Standards and Technology, **1993**.
[32] Désert, A.; Chaduc, I.; Fouilloux, S.; Taveau, J.-C.; Lambert, O.; Lansalot, M.; Bourgeat-Lami, E.; Thill, A.; Spalla, O.; Ravaine, S.; Duguet, E. High-Yield Preparation of Polystyrene/Silica Clusters of Controlled Morphology. *Polymer Chemistry* **2012**, *3* (5), 1130.
[33] Lansade, D.; Lewandowski, S.; Remaury, S.; Perraud, S.; Sierra, G., Solé, S.; Carlotti, S. Ageing improvement of silicon-based resins subject to proton irradiation in spatial geostationary environment. *International Symposium on Materials in Space Environment (ISMSE)*, Oct **2018**, Biarritz, France.
[34] Zhou, L.; Wu, Y.; Liu, G.; Li, Y.; Fan, Q.; Shao, J. Fabrication of High-Quality Silica Photonic Crystals on Polyester Fabrics by Gravitational Sedimentation Self-Assembly. *Coloration Technology* **2015**, *131* (6), 413–423.
[35] Khlebtsov, B. N.; Khanadeev, V. A.; Khlebtsov, N. G. Determination of the Size, Concentration, and Refractive Index of Silica Nanoparticles from Turbidity Spectra. *Langmuir* **2008**, *24* (16), 8964–8970.
[36] Schneider, F.; Draheim, J.; Kamberger, R.; Wallrabe, U. Process and Material Properties of Polydimethylsiloxane (PDMS) for Optical MEMS. *Sensors and Actuators A: Physical* **2009**, *151* (2), 95–99.
[37] Sun, S.; Pan, Z.; Yang, F. K.; Huang, Y.; Zhao, B. A Transparent Silica Colloidal Crystal/PDMS Composite and Its Application for Crack Suppression of Metallic Coatings. *Journal of Colloid and Interface Science* **2016**, *461*, 136–143.

[38] Marco, J.; Remaury, S. Evaluation of Thermal Control Coatings Degradation in Simulated Geo-Space Environment. *High Performance Polymers* **2004**, *16* (2), 177–196.
[39] Stöber, W.; Fink, A.; Bohn, E. Controlled Growth of Monodisperse Silica Spheres in the Micron Size Range. *Journal of Colloid and Interface Science* **1968**, *26* (1), 62–69.
[40] Goodwin, J. W.; Harbron, R. S.; Reynolds, P. A. Functionalization of Colloidal Silica and Silica Surfaces via Silylation Reactions. *Colloid & Polymer Science* **1990**, *268* (8), 766–777.9
[41] Liberman, A.; Mendez, N.; Trogler, W. C.; Kummel, A. C. Synthesis and Surface Functionalization of Silica Nanoparticles for Nanomedicine. *Surface Science Reports* **2014**, *69* (2-3), 132–158.
[42] Zhang, L.; Chang, Z. X.; Li, D. L. The Surface Modification of Silica with Vinyltriethoxysilane. *Advanced Materials Research* **2011**, *399-401*, 1123–1130.
[43] Karstedt, B. D. Platinum complexes of unsaturated siloxanes and platinum containing organopolysiloxanes, U.S. Patent 3,775,452. November 27, **1973**.
[44] European Cooperation for Space Standardization, Measurements of thermo-optical properties of thermal control materials, ECSS-Q-ST-70-09C **2008**.
[45] Huszank, R.; Szikra, D.; Simon, A.; Szilasi, S. Z.; Nagy, I. P., $^{4}He^{+}$ Ion Beam Irradiation Induced Modification of Poly(dimethylsiloxane). Characterization by Infrared Spectroscopy and Ion Beam Analytical Techniques. *Langmuir*, **2011**, *27*, 3842-3848.